Arabian Journal of Chemistry 16 (2023) 105206

Contents lists available at ScienceDirect

Arabian Journal of Chemistry

journal homepage: www.sciencedirect.com

Original article

Fabrication and modification of PVDF membrane by PDA@ZnO for enhancing hydrophilic and antifouling property

Yingjian Zhai, Jing Yang *

School of Urban Planning and Municipal Engineering, Xi'an Polytechnic University, Xi'an 710048, China

ARTICLE INFO

Article history:
Received 8 March 2023
Accepted 13 August 2023
Available online 20 August 2023

Keywords:
PDA@ZnO nanoparticles
PVDF hybrid membrane
Hydrophilicity
Dye rejection
Antifouling performance

ABSTRACT

There is an urgent need for an antifouling membrane to treat the large volume of dye-containing wastewater generated annually by the dyeing and printing industry. PDA@ZnO/PVDF membranes were synthesized by doping polydopamine (PDA) and zinc oxide (ZnO) nanoparticles into the polyvinylidene fluoride (PVDF) membranes via non-solvent induced phase separation (NIPS) method in which polyvinylpyrrolidone (PVP) and lithium chloride (LiCl) were chosen as the porogens respectively. Their microstructures were characterized, and the membranes were examined for antifouling properties and membrane separation performance. The presence of PDA@ZnO nanoparticles on the PVDF membrane was evidenced by X-ray diffraction (XRD), scanning electron microscopy (SEM) and Fourier transform infrared (FTIR) measurements. The addition of PDA@ZnO enhanced the mechanical strength and hydrophilicity of the nanocomposite membranes. The PVDF membranes' water permeability and antifouling properties improved following mixing modification, according to the dye filtration test. The pure water flux of PDA@ZnO/PVDF hybrid membranes changed from 260.0 $L{\cdot}m^{-2}{\cdot}h^{-1}{\cdot}bar^{-1}$ to 1339.2 $L{\cdot}m^{-2}{\cdot}h^{-1}{\cdot}bar^{-1}$ by varying the concentration of PDA@ZnO nanoparticles from 0 wt% to 1.6 wt%. The retention performance of the modified membranes was shown to be significantly superior to the pure PVDF membrane. The modified membranes with the addition of 2.0 wt% PVP and 1.6 wt% PDA@ZnO nanoparticles had highly disperse blue 79 (DB 79) retentions (88.5%), indicating that the modified membrane possessed the characteristics of a promising membrane for the purification of dye. Tests found that PDA@ZnO significantly improved the membrane's antifouling performance.

1. Introduction

One of the most essential resources for human survival is water. Water contamination has emerged as a global issue as a result of the world's rapid economic development and population growth. Globally, the printing and textile industries are responsible for severe water pollution (da Silva et al., 2020). These industries produce a large proportion of wastewater contaminated with dyes. Many dyes are toxic and difficult to degrade. Therefore, the efficient removal of organic dyestuffs has become a vital issue to be addressed in the deep treatment and reuse of dye wastewater.

Because membrane-based separation technology successfully rejects contaminants from wastewater, it has been used in various fields for water treatment (Zhao et al., 2019). Polyvinylidene fluoride (PVDF) is a popular membrane material due to its good mechanical strength, chemical resistance, thermal stability and other properties (Mahdavi et al., 2022). However, pure PVDF membranes are extremely hydrophobic because of the insufficient surface energy of PVDF. High pressure filtration is needed for very hydrophobic membranes because hydrophobic particles that are deposited on the membrane surface or in the membrane pores might seriously clog the membrane (Sun et al., 2020). Therefore, low-contamination PVDF membranes can be created by improving the PVDF membrane's hydrophilicity (Muchtar et al., 2019).

Modified PVDF membranes have become popular in recent years for filtering out dyes and other organics from wastewater. Numerous studies have reported employing polymers, monomers, nanoparticles, plasma treatment, and other modifications to PVDF membranes for dye removal (Gopakumar et al., 2019, Talavari et al., 2020). After 5 h of UV exposure, the PVDF-P(L-DOPA)-ZnO photocatalytic membrane created by Popa et al. (2021)

* Corresponding author.
E-mail address: jingy76@163.com (J. Yang).
Peer review under responsibility of King Saud University.

Production and hosting by Elsevier

https://doi.org/10.1016/j.arabjc.2023.105206
1878-5352/

demonstrated 80% rhodamine B degradation efficiency. Direct yellow 4 and direct blue 14 were removed by PVDF membranes modified with dopamine (DA) and halloysite nanotubes (HNT) to a respective extent of 85% and 93.7% (Zeng et al., 2017). PVDF membranes modified with ionic liquids (ILs) and Na-montmorillonite (Na^+ MMT) removed mango red and methylene blue in the range of 93.2%-99.67% with an FRR of 85.4% (Lv et al., 2023). The PVDF@PDA@ZnO membrane prepared by Wang et al. through surface modification showed good separation performance (separation efficiency and separation flux reached 99.1% and 654 $L{\cdot}m^{-2}{\cdot}h^{-1}$, respectively) for a variety of emulsions with photocatalytic function (Wang et al., 2020). Although these materials have proved promising for dye removal, considerable attempts are still being made to improve the retention and antifouling properties of modified PVDF membranes due to the modified materials' limitations. Additionally, modified membranes' antifouling performance is impacted by nanoparticle-modified materials' low compatibility with organic membranes (Zheng et al., 2021).

The high adherence of polydopamine (PDA) to most organic and inorganic materials is well recognized (Zhou et al., 2020). Additionally, PDA, frequently utilized in PVDF membrane modification, can be created when DA self-polymerizes in an alkaline aqueous solution (Cheng et al., 2019). PDA contains amino and phenolic hydroxyl groups, increasing the hydrophilicity of the modified membrane (Xi et al., 2009). In addition, adding PDA to PVDF membranes can significantly improve the retention of contaminants by the modified membranes. Jiang et al. (2014) prepared a PVDF/PDA hybrid membrane with a rejection rate of over 80% against BSA at 1 bar pressure. It has been shown that the modification of PVDF membranes with PDA can improve the antifouling performance of the PVDF membrane (Li et al., 2018). Additionally, PDA can aid in the uniform dispersion of nanoparticles by immobilizing the ions and assisting nanoparticles in attaching to the base membrane with excellent stability (Nambikkattu et al., 2023).

PDA has strong hydrophilic and adhesive properties and can form coordination bonds with metal oxides. Zhang et al. (2017) used PDA to firmly bind TiO_2 nanoparticles to the surface of a thin film composite membrane. It was shown that nanometals and metal oxides have good adsorption properties for cadmium, arsenic, chromium, uranium, and phosphate. Additionally, under UV light, spray-pyrolyzed TiO_2 and ZnO films may efficiently decompose reactive red 152 and terephthalic acid (Deshpande et al., 2020). Combining PDA and different types of nanoparticles into PVDF membranes can give new properties to the modified membranes, such as adsorption and photocatalytic properties. ZnO nanoparticles are a multifunctional agent that is more promising for wastewater remediation due to their distinctive qualities, which include catalysis, photochemical capabilities, therapeutic effects, fungicidal, antibacterial, and UV filtering (Rambabu et al., 2021). The major disadvantage of ZnO nanoparticles is that they are difficult to be recovered, recycled, and reused. In addition, the agglomeration of ZnO nanoparticles is a challenge. However, PDA can facilitate the dispersion of nanomaterials in the polymer matrix by increasing interfacial interactions (charge transfer, π-stacking, hydrogen bonding interactions and hydrophobic interactions).

Inspired by the reports above, modifying PVDF membranes by combining the advantages of PDA and ZnO nanoparticles provides a new idea for removing dyes from water. However, the PDA and ZnO nanoparticles attached to the PVDF membrane surface by surface coating and surface grafting are easily washed off. A combination of PDA and ZnO can be added to PVDF membranes to prepare a comprehensive hybrid membrane and study their effect on nanocomposite membranes. On the other hand, PVDF hybrid membranes with PDA and ZnO additions have been used for dye removal in relatively few studies (Popa et al., 2021). Lithium chloride (LiCl) increases the membrane's mechanical strength and penetration flow while preventing the formation of macropores (Yuan et al., 2022). Polyvinylpyrrolidone (PVP) improves membrane pore structure and hydrophilicity (Ozekmekci et al., 2021). LiCl and PVP were chosen as the porogens for the preparation of the membranes.

In this research, PDA@ZnO nanoparticles were innovatively added to the PVDF matrix containing different porogens for dye effluent treatment. The surface morphology, chemical composition, hydrophilicity, mechanical strength, permeability and antifouling properties of the hybrid membranes were studied in detail. Furthermore, it is worth mentioning that the prepared PDA@ZnO/PVDF hybrid membranes have excellent results in treating dye wastewater. It also elucidates the retention mechanism and antifouling mechanism of the modified membranes when treating different dye solutions. It is expected to establish a polymeric membrane modification method that can easily and efficiently remove dyes from water.

2. Experimental section

2.1. Materials

PVDF (FR904, MW = 300,000 g/mol) powder was purchased from Shanghai San Aifu Co. Ltd. (China). DA (98%) was purchased from Aladdin Reagent Co. Ltd (China). LiCl (>99%), PVP (MW = 44,000 g/mol), N,N-Dimethylacetamide (DMAc, >99%), disperse blue 79 (DB 79) and reactive orange 5 (RO 5) were purchased from Tianjin Kemiou Chemical Reagent Co. Ltd. (China). Tris(hydroxymethyl) aminomethane hydrochloride (Tris, >99%) obtained from Shanghai Blue Season Reagent Co. Ltd. (China). ZnO nanoparticles (particle size 50 nm) were obtained from Sichuan Xilong Chemical Reagent Co. Ltd. (China).

2.2. Synthesis of PDA@ZnO nanoparticles

First, 1 g of DA was dissolved in 100 mL of Tris in a conical flask for 2 h while magnetically stirring at 25 °C. Then, 1 g of ZnO nanoparticles were dissolved in the conical flask's solution for 24 h at 25 °C with magnetic stirring. The resulting solution was centrifuged, and the black solid was obtained. Next, the black solid was dried at 105 °C. The black solid block was finely ground to the PDA@ZnO nanoparticles.

2.3. Preparation of the PDA@ZnO/PVDF hybrid membranes

The best approach for making fluoropolymer membranes for industrial production is non-solvent induced phase separation (NIPS) (Karkhanechi et al., 2018). The casting solution's polymer-rich phase transforms into the membrane matrix throughout the preparation process, while the polymer-poor phase becomes microporous as the liquid membrane is submerged in a coagulation bath (Rahimi and Mahdavi 2019). The preparation process of PDA@ZnO/PVDF membrane is shown in Fig. 1. In the first step, a certain amount of porogens (2.0 wt% according to the membrane weight) were added to the DMAc solvent, and the mixed solutions were received after stirring. Secondly, a certain amount of synthesized PDA@ZnO nanoparticles were added to the solvent and dispersed under the stirring treatment for 2 h. In the third step, the PVDF powder was poured into the above solution and stirred at 60 °C for 12 h to obtain the homogenous casting solution. Before usage, PVDF powder was dried for 24 h at 60 °C in a vacuum oven. During the fourth step, the air bubbles are removed from the casting solution in a vacuum oven for 24 h. The casting solution was cast on a glass plate, and a membrane maker was used to create

the membrane. The final procedure involved quickly submerging the membranes in deionized water to remove the remaining solution.

Pure PVDF membrane was fabricated using the same procedure, except no PDA@ZnO nanoparticles were added. The membrane thickness was approximately 200 μm. The chemical composition of the PDA@ZnO/PVDF hybrid membranes is shown in Table 1.

2.4. Characterizations

Scanning electron microscopy (SEM, JEOL JSM-6300, Hitachi, Tokyo, Japan) was used to examine the morphologies of the membranes' surfaces and cross-sections at a 5 kV acceleration voltage. A Rigaku D/max-2550 pc X-ray diffractometer (XRD, Rigaku D/max-2550, Hitachi, Tokyo, Japan) with CuK radiation under the settings of 40 kV and 40 mA was used to evaluate the crystal structure of the modified membranes. Fourier transform infrared spectroscopy (FTIR, Nicolet 5700, Thermo Nicolet Corporation, Fitchburg, WI, USA) was used to analyze the modified membranes, and the KBr compression method was used to identify the wavelength measurement range of 400–4000 cm^{-1}. The membrane's surface hydrophilicity was identified by measuring water contact angle (WCA). The WCA of the membrane surface was measured with a contact angle analyzer (JY-82, Chengde Ding Testing Equipment Co. Ltd) at 25 °C. Deionized water is dropped onto the surface of the sample to measure the contact angle (Gopakumar et al., 2019). The WCA for each modified membrane was determined by averaging the measurements for three independent membranes. The mechanical property of the membrane was tested using a tensile strength tester (HK-202A, Dongguan Hengke Automatic Equipment Co. Ltd). The prepared membrane was cut into 80 × 10 mm spline and applied to the tensile test. The machine stretched the sample at a speed of 25.0 mm/min. Each sample had three measurements, and the average value was computed.

The gravimetric method was used to determine the overall porosity (ε) (Ocakoglu et al., 2021). The membrane was desiccated for 24 h before being weighed to determine its weight under dry conditions (W_{dry}). The dried membrane was then divided into squares measuring (40 mm × 40 mm) and submerged in distilled water for five minutes. The membranes were then gently cleansed of any remaining water on their surface using a clean cloth before being weighed (W_{wet}). Using Eq. (1), the produced membrane's overall porosity (ε) was calculated (Sakarkar et al., 2020).

$$\varepsilon = \frac{W_{wet} - W_{dry}}{\rho_w \times A \times L} \times 100\% \quad (1)$$

where ε (%) is the overall porosity, W_{wet} (g) is the weight of the wet membrane, W_{dry} (g) is the weight of the dry membrane, ρ_w (0.998 $g{\cdot}cm^{-3}$) is the density of pure water at room temperature, A (cm^2) is the effective area of the membrane, and L (cm) is the membrane thickness.

Additionally, using data from the pure water flux and porosity, the Guerout-Elford-Ferry Eq. (2) was used to calculate the mean pore radius (r_m) (Tan et al., 2019).

$$r_m = \sqrt{\frac{(2.9 - 1.75\varepsilon) \times 8\mu L J}{\varepsilon \times A \times \Delta P}} \quad (2)$$

where r_m (nm) is the mean pore radius, ε (%) is the overall porosity, A (m^2) is the effective area of the membrane, μ (8.9×10^{-4} Pa·s) is water viscosity, L (m) is the thickness of the membrane, J ($m^3{\cdot}s^{-1}$) is the volume of the permeate water per unit time, ΔP (0.1 MPa) is the operating pressure.

2.5. Filtration tests

2.5.1. Permeability

Our lab-built dead-end ultrafiltration equipment conducts testing on the flux and antifouling of pure water. The permeation test was carried out at 25 °C and 0.1 MPa, and the membrane's effective filtering area was 7.07 cm^2. The permeate flux was pre-compacted with deionized water under 0.15 MPa for each test sample until it stabilized. After lowering the transmembrane pressure, the permeate was measured for 30 min at 0.1 MPa to determine the deionized water flux (Jw). Using Eq. (3), the membrane's pure water flux was determined (Han et al., 2023).

$$J_W = \frac{V}{A \times T \times \Delta P} \quad (3)$$

where J_w ($L{\cdot}m^{-2}{\cdot}h^{-1}{\cdot}bar^{-1}$) is the pure water flux, V (L) is the volume of permeated water for the membranes, A (m^2) is the membrane area, T (h) is the time of recording, ΔP (1 bar) is the operating pressure.

2.5.2. Separation performance

The most popular dyes in the paint and textile industries are reactive and dispersion dyes (Gholami et al., 2022). In this experiment, RO 5 ($C_{26}H_{17}ClN_7Na_3O_{10}S_3$, MW = 788.1 g/mol) and DB 79 ($C_{24}H_{27}BrN_6O_{10}$, MW = 639.4 g/mol) were selected for testing among reactive and disperse dyes, respectively. In the experiments, 50 $mg{\cdot}L^{-1}$ solutions of RO 5 and DB 79 were prepared. The pH of 50 mg/L of RO 5 and DB 79 at 25 °C were 8.04 and 7.8, respectively. The optimum absorbance wavelengths for RO 5 and

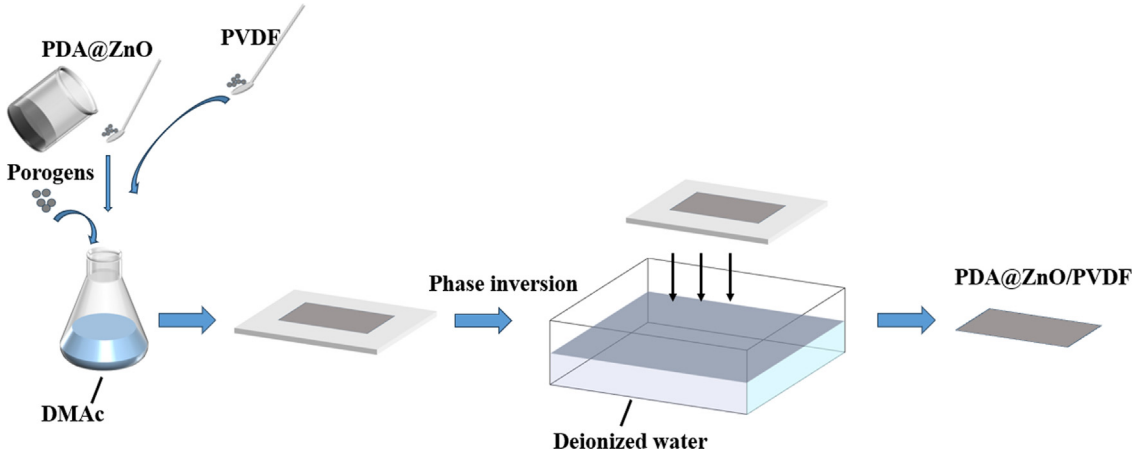

Fig. 1. Schematic illustration of pda@zno/pvdf preparation process.

Table 1
The chemical composition of the PDA@ZnO/PVDF hybrid membranes.

Membrane ID	Porogens	Porogens content (wt%)	PVDF (wt%)	PDA@ZnO (wt%)	DMAc (wt%)
PVDF	–	–	15.0	–	85.0
PVDF(PVP)	PVP	2.0	15.0	–	83.0
PDA@ZnO/PVDF(PVP)-0.4	PVP	2.0	15.0	0.4	82.6
PDA@ZnO/PVDF(PVP)-0.8	PVP	2.0	15.0	0.8	82.2
PDA@ZnO/PVDF(PVP)-1.2	PVP	2.0	15.0	1.2	81.8
PDA@ZnO/PVDF(PVP)-1.6	PVP	2.0	15.0	1.6	81.4
PDA@ZnO/PVDF(PVP)-2.0	PVP	2.0	15.0	2.0	81.0
PVDF(LiCl)	LiCl	2.0	15.0	–	83.0
PDA@ZnO/PVDF(LiCl)-0.4	LiCl	2.0	15.0	0.4	82.6
PDA@ZnO/PVDF(LiCl)-0.8	LiCl	2.0	15.0	0.8	82.2
PDA@ZnO/PVDF(LiCl)-1.2	LiCl	2.0	15.0	1.2	81.8
PDA@ZnO/PVDF(LiCl)-1.6	LiCl	2.0	15.0	1.6	81.4
PDA@ZnO/PVDF(LiCl)-2.0	LiCl	2.0	15.0	2.0	81.0

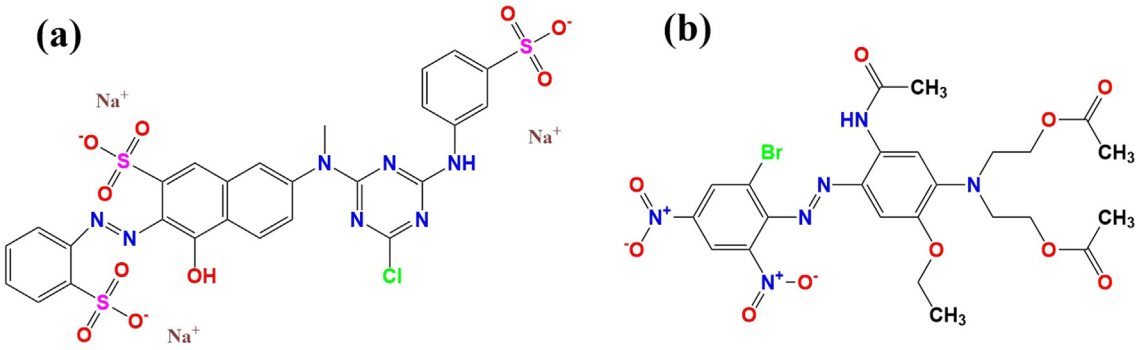

Fig. 2. Chemical structures of (a) RO 5 and (b) DB 79.

DB 79 were 480 nm and 535 nm, respectively. Fig. 2 provides the chemical structures of the colours utilized.

Until the permeate flux achieved a stable value, each test sample was pre-pressurized with the solution under test at a pressure of 0.15 MPa. All membranes were tested at a pressure of 0.1 MPa for 30 min. The dye rejection (R) was calculated using the following Eq. (4) (Sakarkar et al., 2020).

$$R = \left(1 - \frac{C_2}{C_1}\right) \times 100\% \quad (4)$$

where R (%) is the dye rejection, C_1 (mg·L^{-1}) is the concentration of the feed solution, C_2 (mg·L^{-1}) is the concentration of the permeate.

2.6. Antifouling tests

In the experiments, 50 mg·L^{-1} solutions of DB 79 and RO 5 were prepared. The membrane was cut to a size of 4 cm × 4 cm and immersed in 30 mL of dye solution for 24 h at 25 °C. After removing the membrane, a spectrophotometer was used to measure and compute the remaining dye concentration. The adsorption capacity (Q_e, ug·cm^{-2}) was calculated using Eq. (5) (Tan et al., 2019).

$$Q_e = \frac{(C_S - C_F) \times V}{A} \quad (5)$$

where Q_e (ug·cm^{-2}) is the adsorption capacity, C_S (mg·L^{-1}) is the initial concentration of dyes, C_F (mg·L^{-1}) is the dye concentration at the end, A (cm^2) is the effective membrane area, V (L) is the volume of dye solution.

Wash the membrane three times with deionized water to remove reversibly adsorbed dye molecules. In order to maintain a constant flow, the membrane was pressured with deionized water at 0.15 MPa for 30 min. Deionized water, followed by filtration at 0.10 MPa membrane pressure for 30 min, was used to test the membrane's pure water flow recovery (J_2). The following Eq. (6) was used to compute the flux recovery ratio (FRR) degree (Han et al., 2023).

$$FRR = \frac{J_2}{J_1} \times 100\% \quad (6)$$

where FRR (%) is the flux recovery ratio, J_1 (L·m^{-2}·h^{-1}·bar^{-1}) and J_2 (L·m^{-2}·h^{-1}·bar^{-1}) are the pure water flux and the pure water flux recovery of the membrane, respectively.

3. Results and discussion

3.1. Chemical structure analysis

The functional groups of PDA@ZnO, pure PVDF membrane, and PDA@ZnO/PVDF hybrid membranes were analyzed using FTIR spectra and the results are shown in Fig. 3. The strong absorption band at 1181 cm^{-1} and 876 cm^{-1} can be associated with the stretching vibration of —CF_2 (Radwan et al., 2016). The C—C skeleton's stretching vibration is responsible for the absorption peak's appearance in the medium frequency region at 1070 cm^{-1}. (Chen et al., 2021). The representative peak at 1396 cm^{-1} is associated with the deformation vibration of —CH_2 (Van Tran et al., 2019).

The stretching vibrations of the aromatic ring of polydopamine are responsible for a new peak in the modified membrane located at 1630 cm^{-1}. (Nambikkattu et al., 2023). The band's existence is evidence that PDA was effectively incorporated into the modified membrane. PDA can aid in the uniform dispersion of ZnO nanoparticles within the membrane, which is essential for enhancing the membrane's internal structure. The absorption peaks at 3500–2950 cm^{-1} indicate the presence of N—H and O—H bonds, which

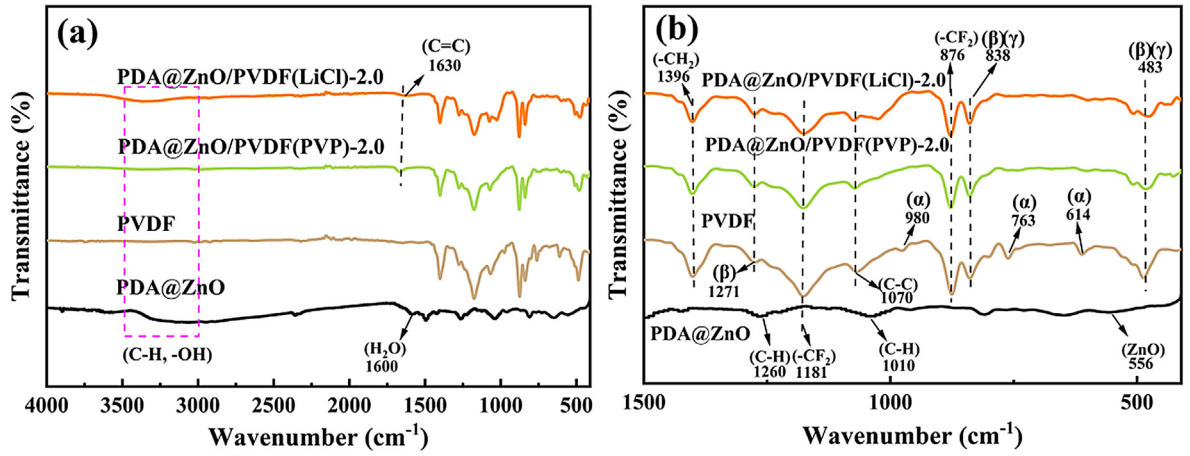

Fig. 3. FTIR spectra of PDA@ZnO nanoparticles, pure PVDF membrane, and PDA@ZnO/PVDF hybrid membranes: (a) 4000–400 cm^{-1}, (b) 1500–400 cm^{-1}.

are essential for the hydrophilicity of the membrane (Popa et al., 2021). The pure PVDF membrane did not exhibit this peak. The spectrum of PDA@ZnO contains a strong absorption band located at the frequency of 556 cm^{-1}, which is typical of the lattice vibrations of ZnO. The C–H bond stretching vibrations at various saturations on the PDA are shown by the peaks at 1260 and 1010 cm^{-1}, respectively. For PDA@ZnO nanoparticles, the broad peak at around 1600 cm^{-1} is due to bending vibrations on H_2O molecules adsorbed on the ZnO nanoparticles. The bending vibration of H_2O molecules on the PDA@ZnO/PVDF hybrid membranes can be seen at 1600 cm^{-1}, which proves the successful preparation of the PDA@ZnO modified PVDF membranes.

FTIR spectroscopy allows the determination of the α-phase, β-phase and γ-phase in PVDF. The characteristic bands at 614 cm^{-1}, 763 cm^{-1} and 980 cm^{-1} are caused by the α-phase (Ike et al., 2017). The absorption bands at 483 cm^{-1}, 838 cm^{-1}, and 1271 cm^{-1} belong to the β phase of crystalline PVDF (Radwan et al., 2016, Ike et al., 2017). The γ phase of crystalline PVDF is represented by the absorption bands at 483 cm^{-1} and 838 cm^{-1} (Eleshmawi 2008). The α-phase absorption peaks of the PVDF membrane at 763 cm^{-1} and 614 cm^{-1} were weakened, probably due to the transformation of the α-phase into the β-phase by adding nanoparticles (Lai et al., 2014). The mechanical properties of membranes are enhanced by stabilizing the β-phase (Popa et al., 2021).

3.2. Phase structure analysis

PDA@ZnO/PVDF hybrid membranes were characterized using XRD to determine their crystalline phases and demonstrate the presence of PDA@ZnO nanoparticles inside the membrane. The crystalline phases of PVDF, which is a semi-crystalline polymer, include α, β, and γ. At room temperature, the α-phase is thought to be the most stable. Fig. 4 displays the XRD spectra of PDA@ZnO nanoparticles, the pure PVDF membrane, and the PDA@ZnO/PVDF hybrid membranes.

The diffraction peaks of the α-phase are located at 18.8°, 21.0°, 38.8°, and 41.4°, corresponding to the reflections of (020), (110), (002), and (111), respectively (Cui et al., 2015). The specific peak of the orthogonal beta phase is located at 20.26°, corresponding to the (110)/(200) reflection (Martins et al., 2014). The specific peaks of the γ phase are located at 18.5°, 20.2°, and 39.4°, corresponding to the (020), (110), and (211) planes (Cai et al., 2017). A supplementary diffraction peak at 2θ = 20.26° is present in the modified membranes, which may be the result of the addition of nanoparticles, which changed the α-phase into the β-phase. The XRD curves

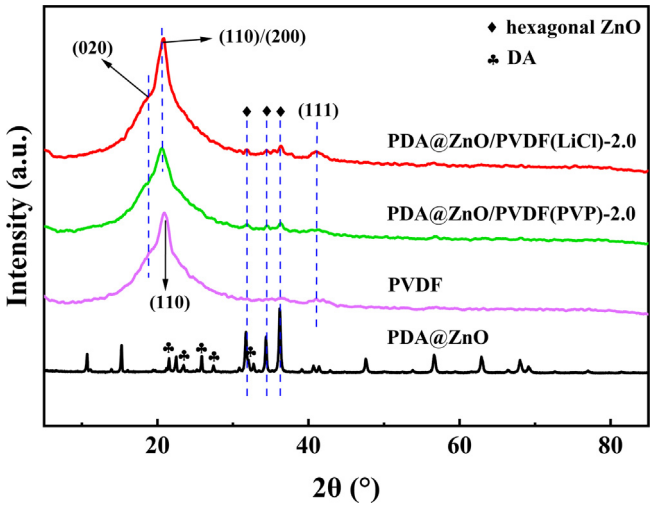

Fig. 4. XRD pattern of PDA, ZnO, PDA@ZnO nanoparticles, pure PVDF membrane, and PDA@ZnO/PVDF hybrid membranes.

of PDA@ZnO nanoparticles and PDA@ZnO/PVDF hybrid membranes showed extra peaks at 2θ = 31.58°, 34.28°, and 36.22° in comparison to pure PVDF membrane, which corresponds to ZnO crystalline phase (Tavakoli et al., 2021). In addition, the DA peaks at 21.5°, 23.18°, 25.86°, 27.3° and 31.98° confirm the crystal structure (Meng et al., 2017). The XRD image of PDA@ZnO nanoparticles shows both the characteristic peaks of PDA and ZnO nanoparticles, proving that ZnO nanoparticles were successfully doped on PDA. Moreover, it shows that the PDA did not cause any destruction during its interaction with ZnO. In addition to unique PVDF patterns, the PDA@ZnO/PVDF hybrid membranes exhibit peaks typical of the hexagonal structure of PDA@ZnO, demonstrating the successful fabrication of the PDA@ZnO modified PVDF membranes. PDA@ZnO/PVDF hybrid membranes' XRD patterns exhibited no appreciable alterations in the crystal structure from those of pure PVDF membranes (Moazeni et al., 2020).

3.3. Morphological analysis

SEM images of pure PVDF membrane and PDA@ZnO/PVDF hybrid membranes with various porogens are shown in Fig. 5. The upper surface of the pure PVDF membrane has pores between 20 and 30 nm. Fig. 5(a-2) shows that the pure PVDF membrane has no obvious pores in the cross-section and has a more disorganized

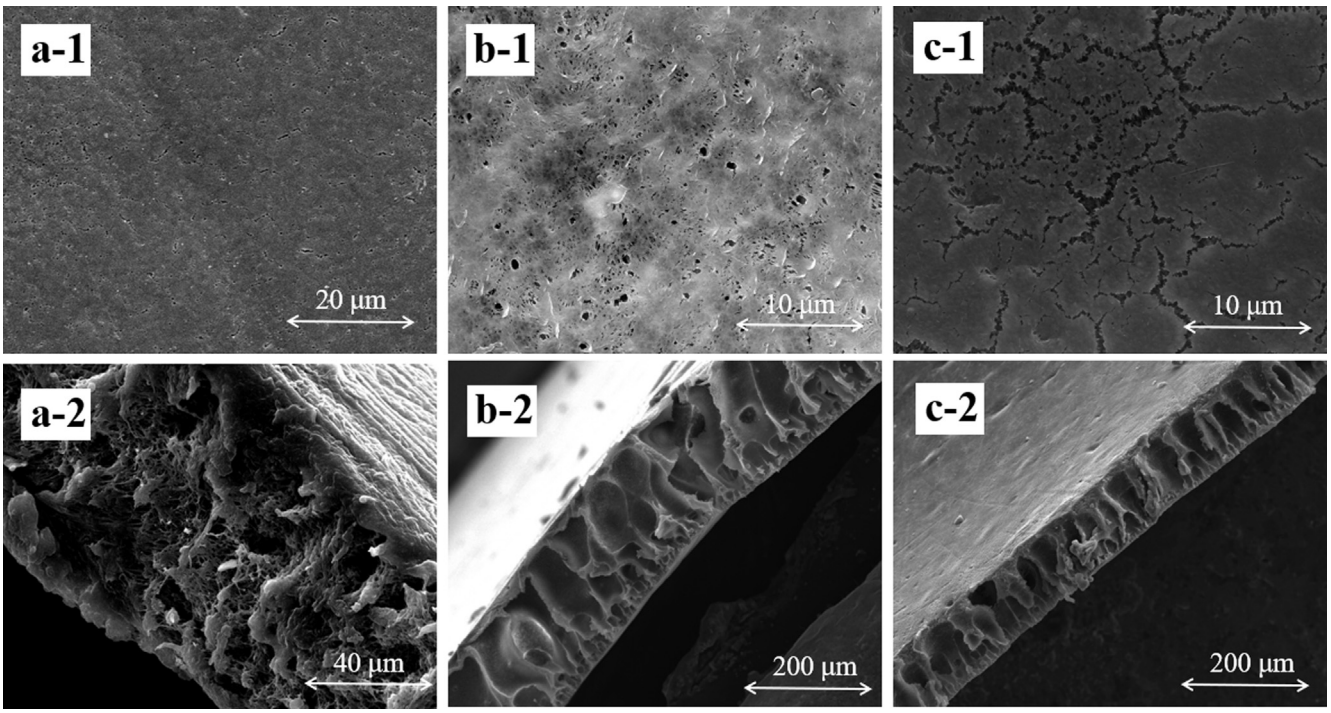

Fig. 5. SEM image of the top surface and cross-section of membranes: (a) pure PVDF membrane, (b) PDA@ZnO/PVDF(PVP)-2.0, (c) PDA@ZnO/PVDF(LiCl)-2.0.

and dense internal structure. Fig. 5(b-1) shows the surface morphology of PDA@ZnO/PVDF(PVP)-2.0. The pore size of the PDA@ZnO/PVDF(PVP)-2.0 surface is 80 nm to 90 nm, and the membrane surface is flat and smooth. The creation of membranes and the size and shape of the pores in PVDF can be affected by the presence of PDA@ZnO, which may also speed up the process of phase separation. PDA and ZnO nanoparticles have strong coordination connections that hold them in place and prevent the nanoparticles from forming big clusters. As seen in Fig. 5(b-2), the PDA@ZnO/PVDF(PVP)-2.0 membrane's cross-sectional images displayed characteristic asymmetric membrane topologies comprising a finger-like sublayer and a selected thin skin layer. It can be concluded from Fig. 5 that PDA@ZnO promotes the formation of a thick spongy layer structure and many finger-like structures within the membrane. In filtration tests, the spongy pores can greatly improve the retention effect, while the finger-shaped pores help the permeating water to pass through quickly. Dopamine's active groups, such as its amino and hydroxyl groups, increase the compatibility between PVDF with the modified nanoparticle (Wang et al., 2017). The membrane's internal structure can be altered by adding PDA@ZnO nanoparticles, improving the retention performance and increasing the flux of pure water.

Fig. 5(c-1) and Fig. 5(c-2) show the surface and cross-sectional morphology of PDA@ZnO/PVDF(LiCl)-2.0, respectively. LiCl contributes to the formation of smaller voids on the membrane surface (Fontananova et al., 2006). The pores on the surface of PDA@ZnO/PVDF(LiCl)-2.0 are 40 nm to 50 nm, and these pores are linked together to form long cracks. The crack-like pores are mainly due to the lack of flexibility of the organic additives in LiCl. When dissolved in a solvent, LiCl does not dissociate like an organic porogens but produces immediately integrated ions. As a result, the phase separation is too rapid, which causes the creation of membrane pores to occur too late. Moreover, LiCl will form a gel when it reacts with the dipole moment on the membrane surface, preventing macropores' growth. In addition, due to the particle form of PDA@ZnO, it is easy to settle in the membrane, causing defects. As shown in Fig. 5(c-2), many finger-like pores with small diameters are formed within the membrane, which further improves the retention of the dye by the membrane. The strong polarity of LiCl promotes the crystallization of PVDF in polymer solutions, resulting in smaller pore sizes in PDA@ZnO/PVDF(LiCl)-2.0.

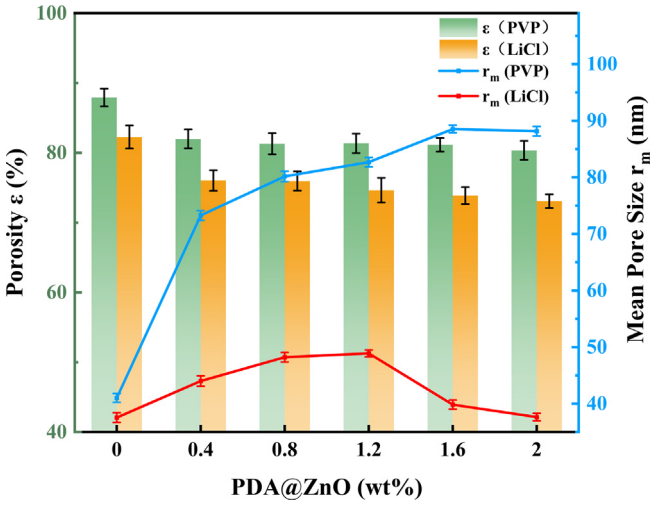

Fig. 6. Porosity (ε) and mean pore size (r_m) of the PDA@ZnO/PVDF hybrid membranes.

3.4. Porosity and mean pore size analysis

Fig. 6 shows the porosity (ε) and mean pore size (r_m) of the PDA@ZnO/PVDF hybrid membranes. The porosity and mean pore size of PVP-added membranes were significantly higher than those of LiCl-added membranes, possibly due to the better pore formation of PVP than LiCl. The morphological analysis of the membranes corroborated this conclusion. Adding more PDA@ZnO does

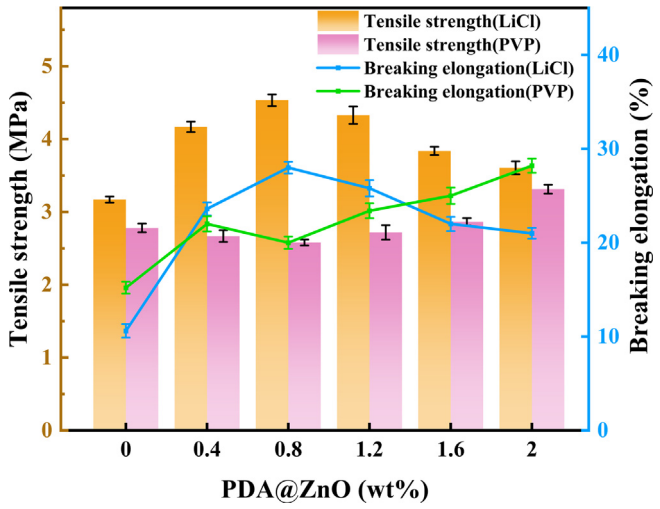

Fig. 7. The mechanical strength of PDA@ZnO/PVDF hybrid membranes.

not appreciably alter the modified membranes' porosity. The addition of PDA@ZnO increased the density of the modified membrane, resulting in a decrease in membrane porosity. The addition of PDA@ZnO increases the modified membrane's mean pore size. When the PDA@ZnO content was 1.6%, the mean pore size of PDA@ZnO/PVDF(PVP)-1.6 reached 88.53 nm and decreased slightly. It indicates that adding PDA@ZnO can increase the mean pore size of the membrane and help improve the internal structure of the PVDF membrane. The mean pore size of LiCl-added membranes increased from 37.55 nm to 48.89 nm as the PDA@ZnO content increased, which may be explained by the small amount of PDA@ZnO improving the membrane's internal structure. However, as the PDA@ZnO content rises, the PDA@ZnO nanoparticles clump together and obstruct the membrane pores, causing the mean pore size to decrease.

3.5. Mechanical strength analysis

Tensile strength and breaking elongation of the pure PVDF membrane and PDA@ZnO modified membranes were shown in Fig. 7. Modified PVDF membranes' pore structure and additives have a significant impact on their mechanical characteristics (Alaa et al., 2021). The tiny pores within the LCl-added membranes improved their mechanical properties. Therefore, the tensile strength of the LiCl membranes is generally higher than that of the PVP-added membranes. The tensile strength of PDA@ZnO/PVDF(LiCl)-0.8 membrane reaches 4.5 MPa. Because LiCl is more brittle than PVP, the PVDF(LiCl) membrane has a lower elongation at break than the PVDF(PVP) membrane. Adding PDA@ZnO can improve the mechanical strength of PVDF membranes. The following reasons were provided: The PVDF molecules and the many hydroxyl groups on the surface of PDA@ZnO could establish hydrogen bonds to increase the mechanical strength of the membrane (Wei et al., 2021). In addition, adding a small amount of PDA@ZnO creates finger-like structures within the membranes that increase tensile strength. However, excessive amounts of PDA@ZnO may result in less cross-linking of the PVDF molecular chains, limiting the membrane's tensile strength mechanically. The PDA@ZnO in the modified membranes can absorb energy in the tensile test, reducing the brittleness of the film. Therefore, the modified membranes had a more excellent elongation at break than the pure PVDF membrane.

3.6. Surface wettability analysis

The WCA measurements were performed to test the membrane's hydrophilicity. According to Fig. 8, there is a slight variation in WCA between the membranes with LiCl and those with PVP added. It indicates that the two porogens have negligible impact on the membranes' hydrophilicity. Fig. 8 demonstrates that the WCA of the modified membranes exhibits a decreasing trend as the amount of PDA@ZnO increases. The WCA of the PVDF(PVP) membrane reduced from 80.1° without PDA@ZnO to 65.4° with 2.0 wt% PDA@ZnO added. The WCA of the PVDF(LiCl) membrane reduced from 77.1° without PDA@ZnO to 66.3° with 2.0 wt% PDA@ZnO added. It could be explained by the fact that the PDA@ZnO nanoparticles include many hydrophilic groups (amino and hydroxyl groups), increasing the membrane's hydrophilicity.

3.7. Filtration performance analysis

Fig. 9 represents the effect of the modification on the pure water flux of the membranes. Under the same operating conditions, all membranes with PVP additions' pure water flux was much larger than those with LiCl additions. It could be attributed to the pore formation effect of better PVP than LiCl. The conclusion is also supported by a study of the modified membranes' pore structures. The combined effects of LiCl and PDA@ZnO reduced the membrane's porosity, reducing the pure water flux.

The pure water flux of the modified membranes was significantly boosted by adding PDA@ZnO to membranes where PVP was chosen as the porogens. In the phase-inversion process, the impact of hydrophilicity on PDA@ZnO accelerated the exchange of non-solvent and solvent, resulting in bigger membrane pores and facilitating water transport. Modified membranes' amino and phenolic hydroxyl groups can also boost membrane flow. The PDA@ZnO/PVDF (PVP)-1.6 membrane achieved a pure water flux of 1339.2 $L{\cdot}m^{-2}{\cdot}h^{-1}{\cdot}bar^{-1}$. The pure water flux of the LiCl-added membranes tends to increase and then decrease with increasing PDA@ZnO content. The modified membrane's internal structure was enhanced by a modest amount of PDA@ZnO, resulting in a larger mean pore size. The modified membranes became denser as more PDA@ZnO was added, which lowered the flux of pure water across the membranes.

The modified membranes' dye rejection abilities were assessed through filtration tests in terms of retention. Fig. 10 shows the mechanism of dye retention by the PDA@ZnO/PVDF membrane. High PVDF membrane retention rates are associated with molecular sieving action and physical separation (Hosseinifard et al., 2020). Anionic dye removal can be improved by modifying the negative membrane's hydrophilicity and surface charge (Khoerunnisa et al., 2020). The anionic dye and the membrane have increased electrostatic attraction, which inhibits the dye molecules from passing through. In addition, the involvement of the OH of the PDA@ZnO nanoparticles and the OH aromatic groups of the dye molecules is another reason for improving the dye removal efficiency. Fig. 11 shows the retention effect of the PDA@ZnO/PVDF hybrid membranes on the dye solution. The retention performance of the LiCl-added membranes is generally higher than that of the PVP-added membranes, as shown in Fig. 11. The retention characteristics of PVP-added and LiCl-added membranes are very different. Large pores develop within the membrane due to PVP, although the development of large pores is inhibited by LiCl (Fontananova et al., 2006). Similar evidence supporting this conclusion was found in the SEM images of the modified membranes. LiCl-added membranes produced more small finger-like pores, significantly improving the retention effect.

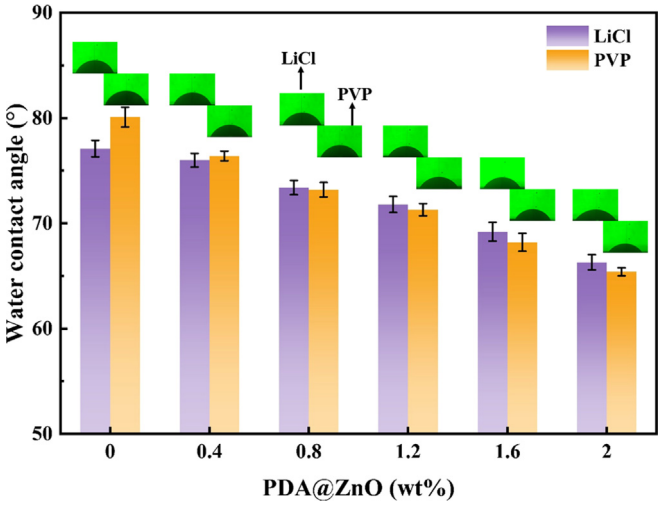

Fig. 8. The WCA of PDA@ZnO/PVDF hybrid membranes.

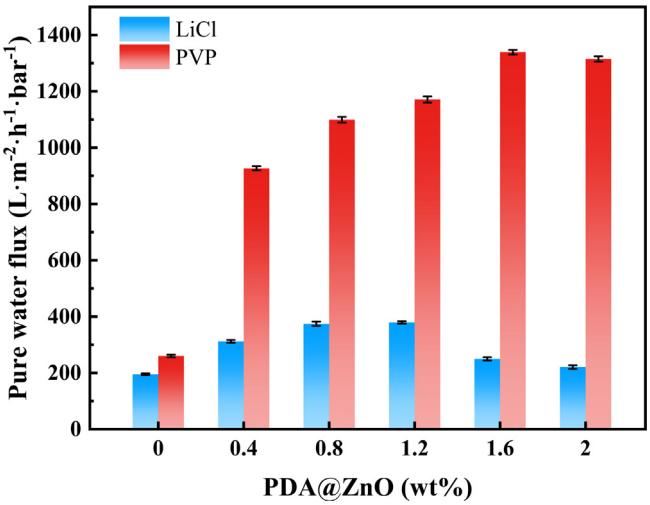

Fig. 9. The pure water flux of PDA@ZnO/PVDF hybrid membranes.

According to Fig. 11, adding PDA@ZnO vastly improved the retention of DB 79 by PDA@ZnO/PVDF hybrid membranes. PDA@ZnO enhances the membrane's hydrophilicity and decreases the interaction of DB 79 molecules with the membrane surface, which prevents dye molecules from penetrating the modified membrane during DB 79 filtering. In addition, adding PDA@ZnO makes the membranes dense and improves the retention of the modified membranes. With a maximum retention of 90.5% for DB 79, the PDA@ZnO/PVDF(LiCl)-1.2 membrane demonstrated good retention. The membranes' structure was optimized throughout the phase change for the LiCl-added membranes due to the joint action of LiCl and PDA@ZnO. During the process, a thicker reticulated sponge layer and regular pores that resemble fingers develop within the membrane, which improves retention.

According to Fig. 11, adding PDA@ZnO enhanced the modified membranes' RO 5 rejection abilities. RO 5 is a highly soluble anionic dye that dissociates in water to produce anions. However, the membrane surface is negatively charged and repels anions. Therefore, forming a layer of dye molecules on the membrane surface is impossible during filtration. Due to the solubility and chemical nature, the molecules of RO 5 easily pass through the membrane, and its retention by the PDA@ZnO/PVDF hybrid membranes is relatively low.

3.8. Antifouling performance analysis

Dye molecules are adsorbed during the membrane's filtration phase, leading to contamination behaviour on the membrane surface. It is necessary to investigate membranes' capability for static adsorption.

Fig. 12 displays the equilibrium adsorption capabilities of the pure PVDF and PDA@ZnO membranes for DB 79 and RO 5. The modified membranes have significantly higher adsorption capacities for DB 79 than RO 5. The modified membranes retained DB 79 more effectively than RO 5. The type of dye has a significant impact on the membrane's ability to adsorb dyes. DB 79 molecules are more readily absorbed in the membrane pores due to their low solubility. As shown in Fig. 12, the LiCl-added membranes had better adsorption capabilities for both dyes than the PVP-added membranes. Numerous surface cracks on the LiCl-added membranes cause increased adsorption of dye molecules by the membrane. As shown in Fig. 12, the adsorption capacities of RO 5 by PDA@ZnO/PVDF hybrid membranes were limited as the PDA@ZnO content increased. The RO 5 molecules may have trouble being

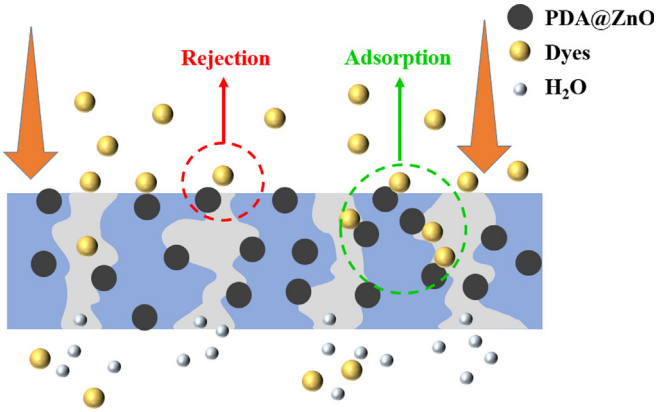

Fig. 10. Schematic illustration of membrane filtration of dyes.

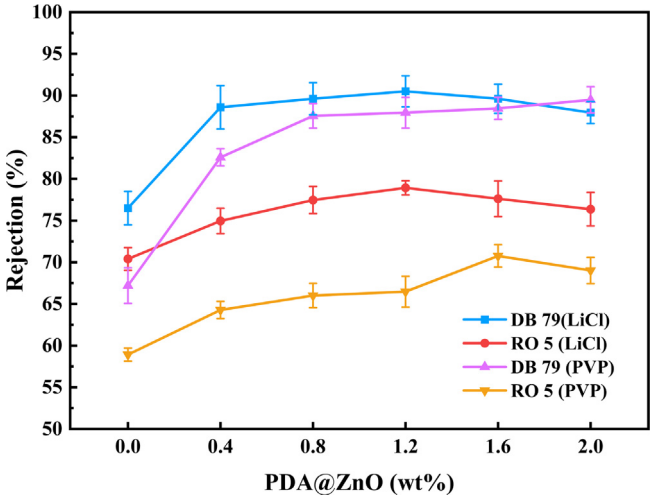

Fig. 11. Dyes rejection of PDA@ZnO/PVDF hybrid membranes.

adsorbed by the membranes as a result of the addition of PDA@ZnO, which causes the pore size of the modified membranes to increase. The addition of PDA@ZnO boosted the adsorption capabilities of DB 79, which may be due to hydrogen bonding and van

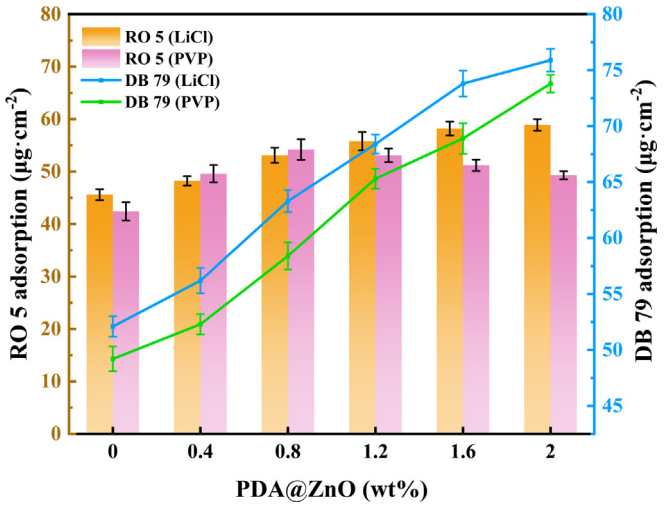

Fig. 12. The comparison of adsorption capacities of different dyes on PDA@ZnO/PVDF hybrid membranes.

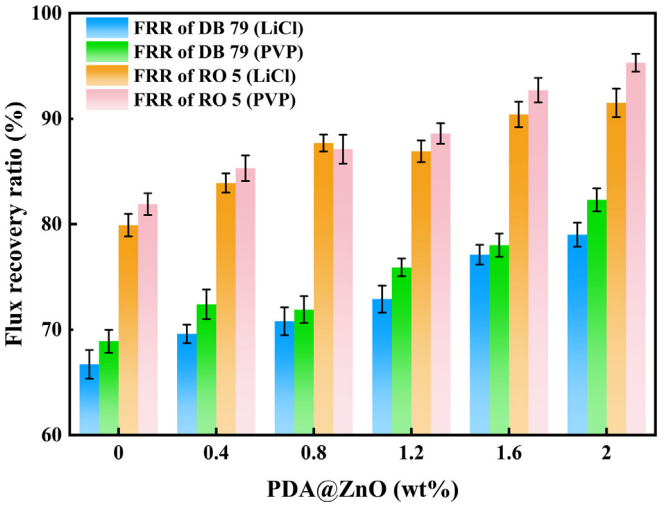

Fig. 13. The flux recovery ration (FRR (%)) of the PDA@ZnO/PVDF hybrid membranes.

der Waals the relationships between DB 79 molecules and the PDA@ZnO/PVDF hybrid membranes (Chen et al., 2020).

Fouling occurs during the time of the separation as a result of the buildup of impurities in the membrane chamber and on the membrane surface. Additionally, hydrogen bonds, electrostatic interactions, and van der Waals bonds all help decrease the membranes' flux (Hassanzadeh et al., 2021). Fig. 13 shows the water flow recovery rates of the PDA@ZnO/PVDF hybrid membranes after filtering two dye solutions separately. As DB 79 molecules are difficult to dissolve in water. They are granular in water and will block the tiny pores in the membrane when they enter. As a result, after DB 79 filtering, the modified membranes' total pure water flow recovery rate is low. The anionic dye (RO 5) was kept on the feed side by an electrostatic repulsion mechanism with an FRR of up to 95.3% because of the modified membrane's electronegativity and hydrophilicity. Numerous studies have shown that if the membrane is hydrophilic, its antifouling performance can be more robust (Lv et al., 2023). Hydrophilic membrane surfaces are more likely to hydrate by forming hydrogen bonds or electrostatic interactions with water molecules. This could result in preferred water molecule adsorption on the membrane surface, eliminating the issue of membrane clogging. The overall trend of increasing FRR indicates that the PDA@ZnO nanoparticles have an excellent antifouling effect. The antifouling performance of the LiCl-added membranes is less than that of the PVP-added membranes, which may be caused by the fact that dye molecules are more easily trapped in the small pores within the membrane. In the SEM analyses, this conclusion is more intuitively reached. The modified membranes can be cleaned and reused after being extremely contaminant-resistant.

3.9. Performance comparison

Until now, the modified PVDF membranes prepared by many researchers have achieved good results in removing dyes and other organics from wastewater. In this work, the PDA@ZnO/PVDF(PVP)-1.6, PDA@ZnO/PVDF(LiCl)-1.6 and pure PVDF membranes and results from prior investigations were compared. The pore size, WCA, tensile strength, pure water flux, rejection, and FRR of several modified PVDF membranes are shown in Table 2.

The best-performing PVDF/ZnO/PDA membrane prepared by Üçel and Demirel showed 97% removal of sodium alginate (SA) and 92% flux recovery, and effective removal of pb^{2+} (Üçel and Demirel 2022). However, the effects of porogens and PDA@ZnO additions on the performance of PVDF membranes have not been investigated. This work adds a certain amount of porogens to the membrane to increase the pore size. Compared to previous investigations, the modified membranes in this one show superior mechanical properties. The PDA@ZnO/PVDF hybrid membranes showed good retention of DB 79, with a retention rate of about 89%. The results of the FRR showed that the PDA@ZnO/PVDF hybrid membranes had high fouling resistance. The overall level of fouling resistance of PDA@ZnO/PVDF hybrid membranes against RO 5 was very high, reaching more than 90%. Compared to pure PVDF membrane, the modified membrane's surface hydrophilicity and water permeability were dramatically increased by adding PDA@ZnO nanoparticles. PVP-added membranes have better properties, such as good pore formation, smoothness and absence of defects. Moreover, the PVP-added membrane possessed a significant flux, which could enhance the treatment efficiency of the membrane for dyes. It was found that PDA@ZnO/PVDF(PVP)-1.6 had the best overall performance. PDA@ZnO/PVDF(PVP)-1.6 achieved a pure water flux of 1339.2 $L{\cdot}m^{-2}{\cdot}h^{-1}{\cdot}bar^{-1}$, a retention rate of about 88.5% of the DB 79, at the same time, had good antifouling properties. Incorporating PDA@ZnO in the membrane significantly improved the FRR of the pure PVDF membrane. The modified membrane can be regenerated by cleaning the membrane surface three times with deionized water when the filtering period is less than 30 min, which is less expensive. When the filtration time is extended, the membrane contamination is aggravated, and the membrane can be cleaned with a low concentration of sodium hypochlorite (Puspitasari et al., 2010) or a solvent with a low concentration of zein (Zhao and Liu 2019). In conclusion, PDA@ZnO/PVDF hybrid membranes are auspicious membrane materials for dye removal. After more testing and research in challenging wastewater treatment environments (Under various PH levels), it is indicated that increased production and utilization of this membrane material could be taken into consideration.

Table 2
Pore size, WCA, tensile strength, pure water flux, rejection and FRR of various PVDF membranes.

Membrane type	Porogens (wt.%)	Pore size (nm)	Tensile strength (MPa)	WCA (°)	Pure water flux ($L{\cdot}m^{-2}{\cdot}h^{-1}$)	Rejection (%)	FRR (%)
PVDF/PDA-TiO_2 (Shi et al., 2023)	–	7.41	1.93	63.6	26.5 (0.1 MPa)	98.7% (Congo red)	70.9
D-A-HNTs/PVDF▲ (Zeng et al., 2017)	PVP (6 wt%)	26.1 ± 0.5	–	59.8 ± 0.4	42.2 (0.1 MPa)	85.0% (Direct yellow 4)	94.3
PVDF/ZnOPb (Ben Dassi et al., 2021)	–	–	–	67.3 ± 0.07	78 (0.12 MPa)	98.9% (Reactive black 5)	–
g-C_3N_4/ZnO(PVDF/PAN) (Veisi et al., 2023)	–	6.47 ± 0.2	–	55.06 ± 0.1	95.8 (0.2 MPa)	78.4% (Methylene blue)	–
PVDF/ZnO/PDA (Üçel and Demirel 2022)	PEG	12.8 ± 0.4	2.15 ± 0.43	–	49 (0.07 MPa)	97% (Sodium alginate)	92
Pure PVDF*	PVP (2 wt%)	41.0 ± 0.8	2.78 ± 0.06	80.1 ± 0.9	260.0 ± 4.2 (0.1 MPa)	67.2% (DB 79), 58.9% (RO 5)	68.9% (DB 79), 81.9% (RO 5)
	LiCl (2 wt%)	37.6 ± 0.9	3.17 ± 0.04	77.1 ± 0.8	195.2 ± 3.1 (0.1 MPa)	76.5% (DB 79), 70.4% (RO 5)	66.7% (DB 79), 79.9% (RO 5)
PDA@ZnO/PVDF*	PVP (2 wt%)	88.5 ± 0.7	2.86 ± 0.05	68.2 ± 0.8	1339.2 ± 8.3 (0.1 MPa)	88.5% (DB 79), 70.8% (RO 5)	78.0% (DB 79), 92.7% (RO 5)
	LiCl (2 wt%)	39.8 ± 0.8	3.83 ± 0.06	69.2 ± 0.9	249.6 ± 6.2 (0.1 MPa)	89.6% (DB 79), 77.6% (RO 5)	77.1% (DB 79), 90.4% (RO 5)

▲ A PVDF membrane is made by mixing halloysite nanotubes (HNTs) with DA and grafting.
* This research.

4. Conclusion

PDA@ZnO/PVDF hybrid membranes were prepared by the NIPS method. The impact of various PDA@ZnO concentrations on the characteristics of modified membranes was examined in this study. The PDA@ZnO nanoparticles were made from PDA and ZnO nanoparticles in a 1 to 1 ratio. PDA helped the ZnO nanoparticles to be uniformly dispersed in the modified membrane. Prepared membranes were characterized by XRD, FTIR and SEM. SEM results demonstrated that PDA@ZnO/PVDF hybrid membrane surface becomes smoother with the introduction of PDA@ZnO nanoparticles. Incorporating PDA@ZnO nanoparticles endowed the modified membrane with distinctly improved surface hydrophilicity and water permeance. It was found that the pure water flux of the PDA@ZnO/PVDF hybrid membrane reached 1339.2 $L{\cdot}m^{-2}{\cdot}h^{-1}{\cdot}bar^{-1}$ when 2.0 wt% PVP and 1.6 wt% PDA@ZnO nanoparticles were added. The PDA@ZnO/PVDF(PVP)-1.6 membrane showed good retention of DB 79 (88.5%), while the overall resistance to contamination of RO 5 (92.7%) was high. In conclusion, PDA@ZnO/PVDF hybrid membranes are auspicious membrane materials for dye removal.

Declaration of Competing Interest

The authors declare that they have no known competing financial interests or personal relationships that could have appeared to influence the work reported in this paper.

Acknowledgement

This research was funded by the Scientific Research Project of Shaanxi province, China (2022SF-287).

References

Alaa, M., Samy, Y., Tawheed, H., et al., 2021. Microstructure and modeling of uniaxial mechanical properties of Polyethersulfone nanocomposite ultrafiltration membranes. Int. J. Mech. Sci. 204.

Ben Dassi, R., Chamam, B., Mericq, J.-P., et al., 2021. Novel polyvinylidene fluoride/lead-doped zinc oxide adsorptive membranes for enhancement of the removal of reactive textile dye. Int. J. Environ. Sci. Technol. 18, 2793–2804.

Cai, X., Lei, T., Sun, D., et al., 2017. A critical analysis of the α, β and γ phases in poly (vinylidene fluoride) using FTIR. RSC Adv. 7, 15382–15389.

Chen, Z., Chen, G.-E., Xie, H.-Y., et al., 2021. Photocatalytic antifouling properties of novel PVDF membranes improved by incorporation of SnO_2-GO nanocomposite for water treatment. Sep. Purif. Technol. 259, 118184.

Chen, Q., Yang, B., Ding, M., et al., 2020. Enhanced physical, mechanical and protein adsorption properties of PVDF composite films prepared via thermally-induced phase separation (TIPS): effect of SiO_2 @PDA nanoparticles. Eur. Polym. J. 140.

Cheng, W., Zeng, X., Chen, H., et al., 2019. Versatile polydopamine platforms: synthesis and promising applications for surface modification and advanced nanomedicine. ACS Nano 13, 8537–8565.

Cui, Z., Hassankiadeh, N.T., Zhuang, Y., et al., 2015. Crystalline polymorphism in poly (vinylidenefluoride) membranes. Prog. Polym. Sci. 51, 94–126.

da Silva, C.C., de Faria Lima, A., Moreto, J.A., et al., 2020. Influence of plasma treatment on the physical and chemical properties of sisal fibers and environmental application in adsorption of methylene blue. Mater. Today Commun. 23, 101140.

Deshpande, B., Agrawal, P., Yenkie, M., et al., 2020. Prospective of nanotechnology in degradation of waste water: a new challenges. Nano-Struct. Nano-Objects 22, 100442.

Eleshmawi, I., 2008. Effect of LiCl filler on the structure and morphology of PVDF films. J. Elastomers Plast. 40, 211–221.

Fontananova, E., Jansen, J.C., Cristiano, A., et al., 2006. Effect of additives in the casting solution on the formation of PVDF membranes. Desalination 192, 190–197.

Gholami, S., Llacuna, J.L., Vatanpour, V., et al., 2022. Impact of a new functionalization of multiwalled carbon nanotubes on antifouling and permeability of PVDF nanocomposite membranes for dye wastewater treatment. Chemosphere 294, 133699.

Gopakumar, D.A., Arumukhan, V., Gelamo, R.V., et al., 2019. Carbon dioxide plasma treated PVDF electrospun membrane for the removal of crystal violet dyes and iron oxide nanoparticles from water. Nano-Struct. Nano-Objects 18, 100268.

Han, D.J., Kim, J.F., Lee, J.-C., et al., 2023. Design of an ionic PVDF-based additive for PVDF water purification membranes with anti-fouling and bactericidal activities. J. Membr. Sci. 121839.
Hassanzadeh, P., Gharbani, P., Derakhshanfard, F., et al., 2021. Preparation and characterization of PVDF/g-C_3N_4/chitosan polymeric membrane for the removal of direct blue 14 dye. J. Polym. Environ. 29, 3693–3702.
Hosseinifard, S.M., Aroon, M.A., Dahrazma, B., 2020. Application of PVDF/HDTMA-modified clinoptilolite nanocomposite membranes in removal of reactive dye from aqueous solution. Sep. Purif. Technol. 251, 117294.
Ike, I.A., Dumée, L.F., Groth, A., et al., 2017. Effects of dope sonication and hydrophilic polymer addition on the properties of low pressure PVDF mixed matrix membranes. J. Membr. Sci. 540, 200–211.
Jiang, J.H., Zhu, L.P., Zhang, H.T., et al., 2014. Improved hydrodynamic permeability and antifouling properties of poly(vinylidene fluoride) membranes using polydopamine nanoparticles as additives. J. Membr. Sci. 457, 73–81.
Karkhanechi, H., Vaselbehagh, M., Jeon, S., et al., 2018. Preparation and characterization of polyvinylidenedifluoride-co-chlorotrifluoroethylene hollow fiber membranes with high alkaline resistance. Polymer 145, 310–323.
Khoerunnisa, F., Rahmah, W., Ooi, B.S., et al., 2020. Chitosan/PEG/MWCNT/Iodine composite membrane with enhanced antibacterial properties for dye wastewater treatment. J. Environ. Chem. Eng. 8, 103686.
Lai, C.Y., Groth, A., Gray, S., et al., 2014. Nanocomposites for improved physical durability of porous PVDF membranes. Membranes 4, 55–78.
Li, J.-H., Ni, X.-X., Zhang, D.-B., et al., 2018. Engineering a self-driven PVDF/PDA hybrid membranes based on membrane micro-reactor effect to achieve super-hydrophilicity, excellent antifouling properties and hemocompatibility. Appl. Surf. Sci. 444, 672–690.
Lv, Z., Xue, P., Xie, T., et al., 2023. High-performing PVDF membranes modified by Na + MMT/ionic liquids (ILs) with different chain lengths: dye adsorption and separation from O/W emulsion. Sep. Purif. Technol. 305, 122516.
Mahdavi, H., Zeinalipour, N., Kerachian, M.A., et al., 2022. Preparation of high-performance PVDF mixed matrix membranes incorporated with PVDF-g-PMMA copolymer and GO@SiO_2 nanoparticles for dye rejection applications. J. Water Process Eng. 46, 102560.
Martins, P., Lopes, A., Lanceros-Mendez, S., 2014. Electroactive phases of poly (vinylidene fluoride): determination, processing and applications. Prog. Polym. Sci. 39, 683–706.
Meng, R., Chen, Y., Zhang, X., et al., 2017. Synthesis of a hydrophilic α-sulfur/PDA composite as a metal-free photocatalyst with enhanced photocatalytic performance under visible light. J. Macromol. Sci. A 54, 334–338.
Moazeni, N., Sadrjahani, M., Merati, A.A., et al., 2020. Effect of stimuli-responsive polydiacetylene on the crystallization and mechanical properties of PVDF nanofibers. Polym. Bull. 77, 5373–5388.
Muchtar, S., Wahab, M.Y., Mulyati, S., et al., 2019. Superior fouling resistant PVDF membrane with enhanced filtration performance fabricated by combined blending and the self-polymerization approach of dopamine. J. Water Process Eng. 28, 293–299.
Nambikkattu, J., Thomas, A.A., Kaleekkal, N.J., et al., 2023. ZnO/PDA/Mesoporous Cellular Foam Functionalized Thin-Film Nanocomposite Membrane towards Enhanced Nanofiltration Performance. Membranes 13, 486.
Ocakoglu, K., Dizge, N., Colak, S.G., et al., 2021. Polyethersulfone membranes modified with CZTS nanoparticles for protein and dye separation: Improvement of antifouling and self-cleaning performance. Colloids Surf. A Physicochem. Eng. Asp. 616, 126230.
Ozekmekci, M., Unlu, D., Copur, M., 2021. Removal of boron from industrial wastewater using PVP/PVDF blend membrane and GO/PVP/PVDF hybrid membrane by pervaporation. Korean J. Chem. Eng. 38, 1859–1869.
Popa, A., Toloman, D., Stefan, M., et al., 2021. Hybrid PVDF-P (L-DOPA)-ZnO membranes for dyes and antibiotics removal through simultaneous action of adsorption and photocatalysis processes. J. Environ. Chem. Eng. 9, 106812.
Puspitasari, V., Granville, A., Le-Clech, P., et al., 2010. Cleaning and ageing effect of sodium hypochlorite on polyvinylidene fluoride (PVDF) membrane. Sep. Purif. Technol. 72.
Radwan, A.B., Mohamed, A.M., Abdullah, A.M., et al., 2016. Corrosion protection of electrospun PVDF–ZnO superhydrophobic coating. Surf. Coat. Technol. 289, 136–143.
Rahimi, A., Mahdavi, H., 2019. Zwitterionic-functionalized GO/PVDF nanocomposite membranes with improved anti-fouling properties. J. Water Process Eng. 32, 100960.
Rambabu, K., Bharath, G., Banat, F., et al., 2021. Green synthesis of zinc oxide nanoparticles using Phoenix dactylifera waste as bioreductant for effective dye degradation and antibacterial performance in wastewater treatment. J. Hazard. Mater. 402, 123560.
Sakarkar, S., Muthukumaran, S., Jegatheesan, V., 2020. Evaluation of polyvinyl alcohol (PVA) loading in the PVA/titanium dioxide (TiO2) thin film coating on polyvinylidene fluoride (PVDF) membrane for the removal of textile dyes. Chemosphere 257, 127144.
Shi, Y., Chen, X., Wu, Q., et al., 2023. Enhance organic pollutants removal of wastewater by a PVDF/PDA-TiO_2 composite membrane with photocatalytic property. J. Environ. Chem. Eng. 110389.
Sun, J., Li, S., Ran, Z., et al., 2020. Preparation of Fe_3O_4@ TiO_2 blended PVDF membrane by magnetic coagulation bath and its permeability and pollution resistance. J. Mater. Res. Technol. 9, 4951–4967.
Talavari, A., Ghanavati, B., Azimi, A., et al., 2020. Preparation and characterization of PVDF-filled MWCNT hollow fiber mixed matrix membranes for gas absorption by Al_2O_3 nanofluid absorbent via gas–liquid membrane contactor. Chem. Eng. Res. Des. 156, 478–494.
Tan, Y., Sun, Z., Meng, H., et al., 2019. A new MOFs/polymer hybrid membrane: MIL-68 (Al)/PVDF, fabrication and application in high-efficient removal of p-nitrophenol and methylene blue. Sep. Purif. Technol. 215, 217–226.
Tavakoli, S., Kharaziha, M., Nemati, S., 2021. Polydopamine coated ZnO rod-shaped nanoparticles with noticeable biocompatibility, hemostatic and antibacterial activity. Nano-Struct. Nano-Objects 25, 100639.
Üçel, İ.S., Demirel, E., 2022. Modification of PVDF membranes using dopamine/zinc oxide for lead removal from aqueous media. Open Journal of Nano. 7, 53–73.
Van Tran, T.T., Kumar, S.R., Lue, S.J., 2019. Separation mechanisms of binary dye mixtures using a PVDF ultrafiltration membrane: Donnan effect and intermolecular interaction. J. Membr. Sci. 575, 38–49.
Veisi, P., Dorraji, M.S.S., Vatanpour, V., et al., 2023. Dimensional effect of ZnO-g-C_3N_4 heterostructures on hydrophilic and anti-fouling properties of the PVDF/PAN composite membrane: dye rejection. J. Environ. Chem. Eng. 110249.
Wang, X., Cong, S., Ma, J., 2017. A biomimetic strategy for improving activity of nano zero-valent iron based on the adhesive behavior of polydopamine on PVDF Al_2O_3 film. Mater. Chem. Phys. 197, 215–225.
Wang, Q., Cui, J., Xie, A., et al., 2020. PVDF composite membrane with robust UV-induced self-cleaning performance for durable oil/water emulsions separation. J. Taiwan Inst. Chem. Eng. 110, 130–139.
Wei, W., Xin, X., Zhichao, Z., et al., 2021. Study on the improvement of PVDF flat ultrafiltration membrane with MWCNTs-OH as the additive and the influence of different MWCNTs-OH scales. Colloid Interface Sci. Commun. 43.
Xi, Z.-Y., Xu, Y.-Y., Zhu, L.-P., et al., 2009. A facile method of surface modification for hydrophobic polymer membranes based on the adhesive behavior of poly (DOPA) and poly (dopamine). J. Membr. Sci. 327, 244–253.
Yuan, A., Yang, J., Mu, R., et al., 2022. Surface free energy, microstructure and performance of polyvinylidene fluoride (PVDF) membrane: the influence of hydrophilic porogens. Ferroelectrics 595, 60–72.
Zeng, G., Ye, Z., He, Y., et al., 2017. Application of dopamine-modified halloysite nanotubes/PVDF blend membranes for direct dyes removal from wastewater. Chem. Eng. J. 323, 572–583.
Zhang, R.-X., Braeken, L., Liu, T.-Y., et al., 2017. Remarkable anti-fouling performance of TiO_2-modified TFC membranes with mussel-inspired polydopamine binding. Appl. Sci.-Basel 7. https://doi.org/10.3390/app7010081.
Zhao, J., Han, H., Wang, Q., et al., 2019. Hydrophilic and anti-fouling PVDF blend ultrafiltration membranes using polyacryloylmorpholine-based triblock copolymers as amphiphilic modifiers. React. Funct. Polym. 139, 92–101.
Zhao, X., Liu, C., 2019. Efficient preparation of a novel PVDF antifouling membrane based on the solvent-responsive cleaning properties. Sep. Purif. Technol. 210.
Zheng, H., Wang, D., Sun, X., et al., 2021. Surface modified by green synthetic of Cu-MOF-74 to improve the anti-biofouling properties of PVDF membranes. Chem. Eng. J. 411, 128524.
Zhou, Z., Zheng, B., Gu, Y., et al., 2020. New approach for improving anticorrosion and biocompatibility of magnesium alloys via polydopamine intermediate layer-induced hydroxyapatite coating. Surf. Interfaces 19, 100501.